Journal of Power Sources 205 (2012) 201–206

Contents lists available at SciVerse ScienceDirect

Journal of Power Sources

journal homepage: www.elsevier.com/locate/jpowsour

Binary oxide-doped Pt/RuO_2–SiO_x/C catalyst with high performance and self-humidification capability: The promotion of ruthenium oxide

Qiao Zeng, Liping Zheng, Jianhuang Zeng, Shijun Liao*

School of Chemistry and Chemical Engineering, South China University of Technology, Guangdong Key Lab for Fuel Cell Technology & Key Lab of Enhanced Heat Transfer and Energy Conservation, Ministry of Education, Guangzhou 510641, China

ARTICLE INFO

Article history:
Received 9 November 2011
Received in revised form 7 January 2012
Accepted 12 January 2012
Available online 21 January 2012

Keywords:
Doped carbon black
Multifunctional catalyst
Non-humidification
Ruthenium oxide
Fuel cell

ABSTRACT

A multifunctional catalyst for fuel cell applications, Pt/RuO_2–SiO_x/C, has been prepared by supporting platinum nanoparticles on surface-modified carbon black, fabricated by in situ hydrolysis of ruthenium and silicon precursors on pre-treated carbon black. The catalyst is extensively characterized by X-ray diffraction, transmission electron microscopy, and X-ray photoelectron spectroscopy. The catalyst shows high activity toward methanol oxidation and oxygen reduction at room temperature. Notably, the addition of ruthenium oxide significantly improves the performance of MEAs under non-humidified conditions. The self-humidification performance of MEAs prepared with Pt/RuO_2–SiO_x/C (using optimized 3 wt.% RuO_2) as the anode catalyst is enhanced by over 20% compared to MEAs prepared with Pt/SiO_x/C as the anode catalyst. It is suggested that the promotion of RuO_2 may result from the high dispersion of platinum caused by adding ruthenium oxide, and the synergistic effect of ruthenium oxide.

1. Introduction

Proton electrolyte membrane fuel cells (PEMFCs) have been used in many stationary and mobile applications in recent years. Although PEMFCs have distinct advantages over their counterparts, such as lithium batteries, their high cost imposes limitations in many instances. Significant breakthroughs to reduce cost, enhance durability, and simplify the system are therefore necessary before this technology can be fully commercialized [1,2]. As is well known, the membrane in a PEMFC system requires water to maintain its proton conductivity during operation. To wet the Nafion ionomer in the membrane, significant energy is consumed in humidifying the anode and cathode gases, which has stimulated research into the development of non-humidifying or self-humidifying membrane electrode assemblies (MEAs) [3–5].

At present, researchers have developed two mainstream methods to achieve non-humidification or self-humidification. One is to modify the membrane by either adding hygroscopic materials, such as silica, zirconia particles, or Pt catalysts (for water production) [6–8], or adding both hygroscopic and Pt catalysts [9–11]. Modifying the membrane using a Pt catalyst is costly, and may create electron-conducting paths that increase the possibility of short circuits through the membrane. To avoid this, a series of multilayer composite membranes and oxide-supported Pt catalyst hybrid membranes have been proposed [12,6,13], but the stability and durability of these composite membranes is still questionable.

Another method to achieve non-humidification or self-humidification is to modify the electrodes by adding hygroscopic materials, such as SiO_2 or Al_2O_3, instead of modifying the membrane, thereby improving the MEA's wettability and performance in conditions of low or no humidity [14–16]. Jung et al. [17,18] investigated water management in MEAs by adding hydrophilic SiO_2 into the catalyst layer under low-humidity conditions, and found this approach was useful for obtaining self-humidifying MEAs. However, SiO_2 particles are easily detached or aggregated in a working MEA, since these hygroscopic oxides are simply mixed (not anchored in the electrodes), consequently lowering cell performance in the long run. Previously in our group [19,20], we attempted to fabricate a self-humidifying MEA by using a composite anode catalyst, Pt/SiO_x/C, which was prepared by modifying a carbon support with ethyl silicate, followed by controllable hydrolysis of the ethyl silicate and deposition of platinum nanoparticles on the silica-modified support. The MEA prepared with this Pt/SiO_x/C catalyst as the anode showed much better self-humidification performance than similar previously reported MEAs. However, the performance was still not adequate to meet the requirements for industrial applications.

To further improve the performance of Pt/SiO_x/C, we attempted to modify a carbon support using a binary oxide rather than only a silica. We found that the addition of ruthenium could significantly

* Corresponding author. Tel.: +86 20 8711 2977; fax: +86 20 8711 3586.
E-mail address: chsjliao@scut.edu.cn (S. Liao).

0378-7753/$ – see front matter © 2012 Elsevier B.V. All rights reserved.
doi:10.1016/j.jpowsour.2012.01.085

enhance the self-humidification performance of $Pt/SiO_x/C$, as well as enhance the catalytic activity toward the anodic oxidation of methanol and the cathodic reduction of oxygen.

2. Experimental

2.1. Catalyst preparation

A typical process was used to prepare the RuO_2–SiO_x/C composite support, involving the following steps. First, XC-72R carbon black (Cabot) was pre-treated in a mixture of hydrogen peroxide and nitric acid, then washed with deionized water and dried at 110 °C. The pretreated XC-72R carbon black was then put into an ethanol solution containing TEOS and $RuCl_3$, and stirred at room temperature to initiate the reaction. Second, the impregnated mixture was placed in an oil bath at 80 °C to induce hydrolysis of the TEOS and $RuCl_3$ as well as evaporation of the solvent, followed by calcination at 350 °C in a nitrogen shielded environment for 5 h to improve the immobilization of the silica and ruthenium oxide on the carbon surface [21]. Finally, Pt/RuO_2–SiO_x/C catalysts were prepared using an organic colloid method [22] that resulted in high Pt dispersion and high catalytic performance. To investigate the effects of the catalysts' ruthenium oxide content, Pt/RuO_2–SiO_x/C with 0, 1, 2, 3, and 5 wt.% ruthenium oxide and 6 wt.% SiO_x were prepared (the choice of 6 wt.% SiO_x was based on our previous work [19,20]); the catalysts were denoted as PRSC0 (P for platinum, R for ruthenium, S for silica, and 0 for the weight percentage of ruthenium oxide content), PRSC1, PRSC2, PRSC3, and PRSC5, respectively. The Pt loading in all catalysts was kept at 20 wt.%.

2.2. Catalyst characterization

The catalysts were observed using a transmission electron microscope (TEM) (JEOL JEM-2010HR, Japan) operated at 200 kV. X-ray powder diffraction (XRD) analysis was carried out with a Shimadzu XD-3A (Japan) using filtered Cu Kα radiation at 35 kV and 30 mA. X-ray photoelectron spectroscopy (XPS) data were obtained with an Axis Ultra DLD X-ray photoelectron spectrometer (Kratos, USA). The binding energies (BEs) were calibrated using the C_{1s} graphite peak at 284.6 eV as the reference. The wetting property of the MEAs was obtained with an OCA 40 video-based automatic contact angle meter (Dataphysics, Germany) by dropping 5 ml pure water onto the MEAs.

2.3. Electrochemical evaluation of the catalysts

The catalysts were evaluated electrochemically by cyclic voltammetry (CV) and linear sweep voltammetry (LSV) using an IM6e electrochemical work station (Zahner, Germany) at room temperature. The electrolytes were 0.5 M H_2SO_4 (either N_2-purged or O_2-saturated) and 0.50 M H_2SO_4 + 0.50 M CH_3OH solutions. A conventional three-electrode electrochemical cell was used for the measurements. A Pt wire and an Ag/AgCl electrode (the latter saturated in KCl) were used as the counter and reference electrodes, respectively. To prepare the working electrode, 5 mg catalyst was dispersed ultrasonically in 1 ml Nafion/ethanol (0.25 wt.% Nafion) for 30 min; then 5 μl ink was pipetted on the 5 mm diameter glassy carbon surface, followed by drying in air, then in an oven at 70 °C for 1 min.

2.4. MEA preparation and performance testing

All MEAs used in this study were prepared using the catalyst spray technique [23]. Catalyst inks were prepared by dispersing catalyst powder into a mixture of isopropanol and 5 wt.% Nafion ionomer solution (DuPont, USA). The mixture was ultrasonicated for 30 min before usage. Nafion 212 membranes were successively pre-treated with 5 wt.% H_2O_2, de-ionized water, 0.5 M H_2SO_4 and de-ionized water at 80 °C for 30 min [20]. The inks were then sprayed on both sides of pre-treated Nafion 212 membrane (DuPont, USA) to form the catalyst layers.

Previous studies on self-humidifying MEAs showed that the increased wettability of the cathode catalyst layer had an adverse effect on cell performance due to flooding. For this reason, commercial Johnson Matthey (JM) HiSPEC-4100 Pt/C catalyst (40 wt.% Pt) was used in the cathodes of all MEAs. The Pt/RuO_2–SiO_x/C composite catalysts were used only in the anodes of our self-humidifying MEAs. The active surface area of both electrodes was 5 cm^2 and the Pt loadings at the anode and cathode were 0.1 and 0.2 mg cm^{-2}, respectively. For a fair comparison, a MEA was prepared using JM 40 wt.% Pt/C catalyst at both anode and cathode.

The MEAs were evaluated in a single cell using a fuel cell testing system (Arbin Instruments, USA). High-purity hydrogen and air were fed into the anode and cathode at flow rates of 300 cm^3 min^{-1} for hydrogen and 800 cm^3 min^{-1} for air (H_2/air stoichiometry: 2/5.3). Before performance measurements, the MEAs were activated at 70 °C in discharge mode for 3 h under 100% humidification conditions. For the non-humidified MEA, the performance was evaluated at 50 °C without humidification, and the back-pressure of both gases was held at 20 psig.

3. Results and discussion

The XRD patterns of the RuO_2–SiO_x/C (3 wt.% RuO_2) supports are shown in Fig. 1A. No peaks associated with silica or ruthenium oxide are observable, indicating that they existed in an amorphous state, possibly immobilized on the carbon surface.

Fig. 1B shows the XRD patterns of Pt/RuO_2–SiO_x/C catalysts with or without different ruthenium content. Compared with the $Pt/SiO_x/C$ catalyst, the Pt(1 1 1) peak of the Pt/RuO_2–SiO_x/C catalysts was very broad, whereas the Pt(2 0 0) and Pt(2 2 0) peaks were almost undetectable, suggesting that Pt was highly dispersed on the support surface. Notably, the Pt diffraction peaks flattened as ruthenium oxide content increased (from 1 wt.% to 3 wt.%), an indication of improved Pt dispersion or downsized Pt particles. As the ruthenium oxide content increased further to 5 wt.%, the intensity of the Pt diffraction peak increased slightly. The average Pt particle sizes for the RuO_2 doped catalysts, as calculated from the Pt(1 1 1) peak using the Scherrer equation [24], were 2.7, 2.4, 2.2, and 2.5 nm for PRSC1, PRSC2, PRSC3, and PRSC5, respectively. Comparing these figures to the Pt particle size of 3.2 nm for the PRSC0 catalyst, it is clear that the addition of ruthenium oxide effectively improved the dispersion of active platinum components. The optimal amount to add seems to be 3.0 wt.%.

Fig. 2 presents TEM images of the Pt/RuO_2–SiO_x/C catalysts containing 3 wt.% ruthenium oxide (PRSC3). It can be seen that the active components are highly dispersed and the average Pt particle size is ca. 2.4 nm, in fair agreement with the above-mentioned XRD observations. It is important that the RuO_2 and SiO_x in the carbon support cannot be observed in the TEM images, as this implies that the oxides may be highly dispersed on the carbon surface, or even molecularly immobilized on the carbon support surface.

Table 1 shows the XPS analysis results for the Pt/RuO_2–SiO_x/C (3 wt.% RuO_2) catalyst (PRSC3) and the RuO_2–SiO_x/C supports. The XPS spectra for Si and Ru in PRSC3 are shown in Fig. 3. Compared with the literature findings, the binding energies of Si and Ru shifted positively (as shown in Table 1). In comparison with pure RuO_2, the Ru_{3p} BE increased from 462.4 to 463.9 eV in PRSC3 (+1.5 eV) and from 462.4 to 463.2 eV in the RuO_2–SiO_x/C supports (+0.8 eV), indicating strong interactions between Ru and others elements in

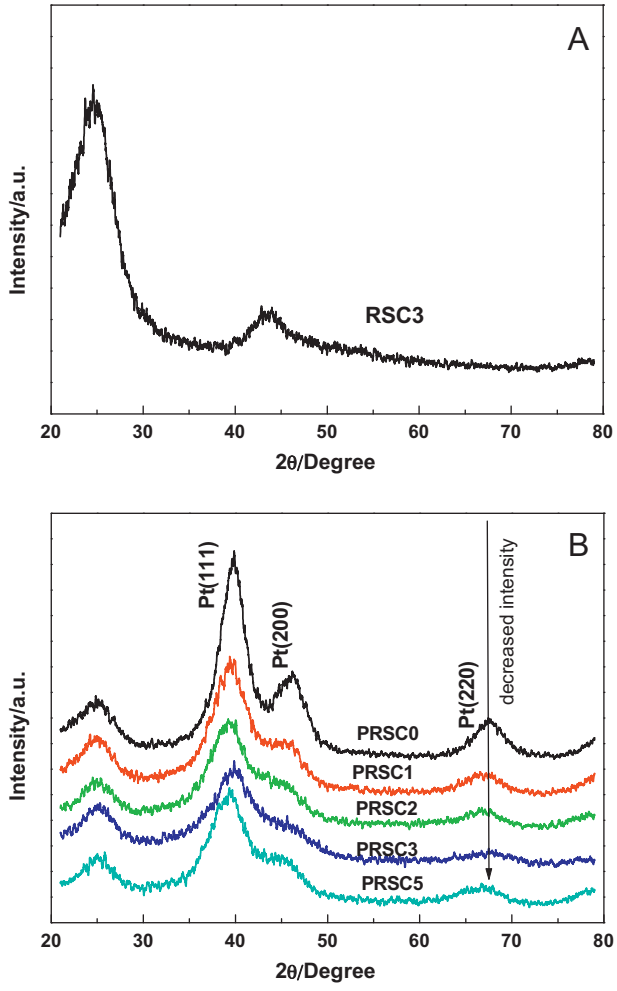

Fig. 1. X-ray diffraction patterns of (A) RuO_2–SiO_x/C support (3 wt.% RuO_2) and (B) Pt/RuO_2–SiO_x/C catalysts with or without different ruthenium oxide content.

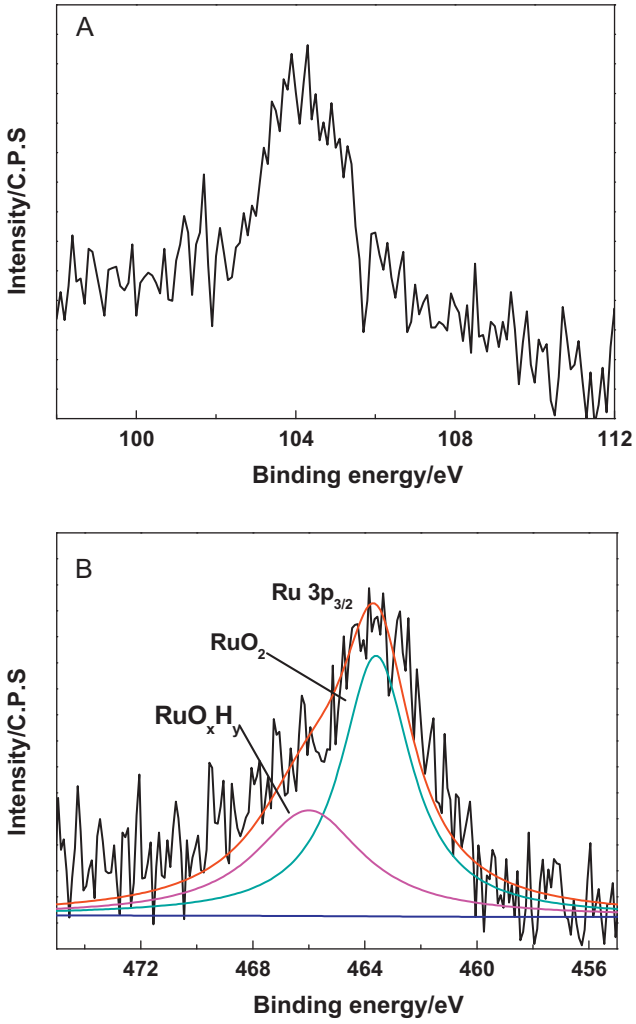

Fig. 3. XPS spectra of (A) Si and (B) Ru of Pt/RuO_2–SiO_2/C catalyst (PRSC3).

the catalyst, or indicating that the Ru atoms may have been incorporated into the Si lattice.

The Ru_{3p} spectra of PRSC3 are shown in Fig. 3B. The Ru_{3p} at 463.9 eV is deconvoluted into doublets of different intensities. The signal at about 463.6 eV can be assigned to oxidized Ru(IV), particularly anhydrous RuO_2. The other component, which is located at a higher BE (about 466 eV), can be associated with hydrous RuO_2 or RuO_xH_y, since its BE is comparatively higher than that of the anhydrous structure [25]. RuO_xH_y plays an important role in the electrocatalytic oxidation of alcohols, due to its high electron and proton conductivity.

Compared with the binding energy of Si in SiO_x, the binding energies of Si in Pt/RuO_2–SiO_x/C (PRSC3) and RuO_2–SiO_x/C increased from 101.9 to 104.3 eV and 103.2 eV, respectively. The

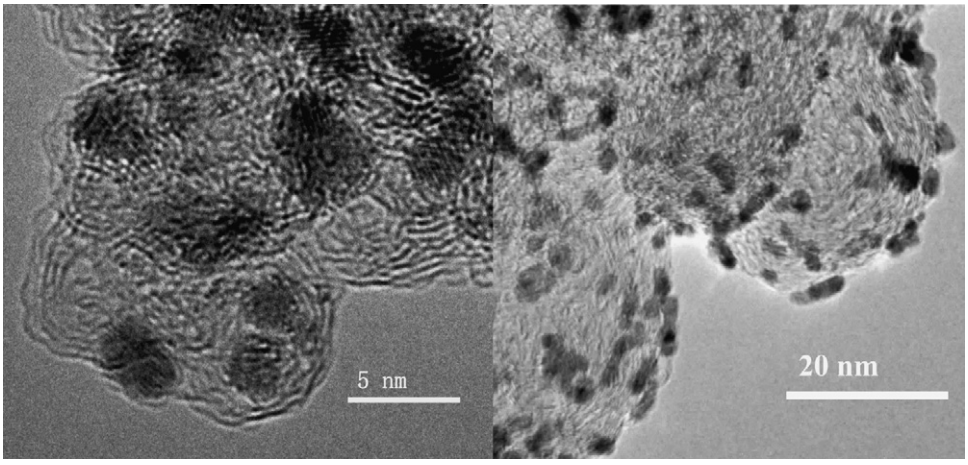

Fig. 2. TEM images of Pt/RuO_2–SiO_x/C catalyst with 3.0 wt.% ruthenium oxide content (PRSC3).

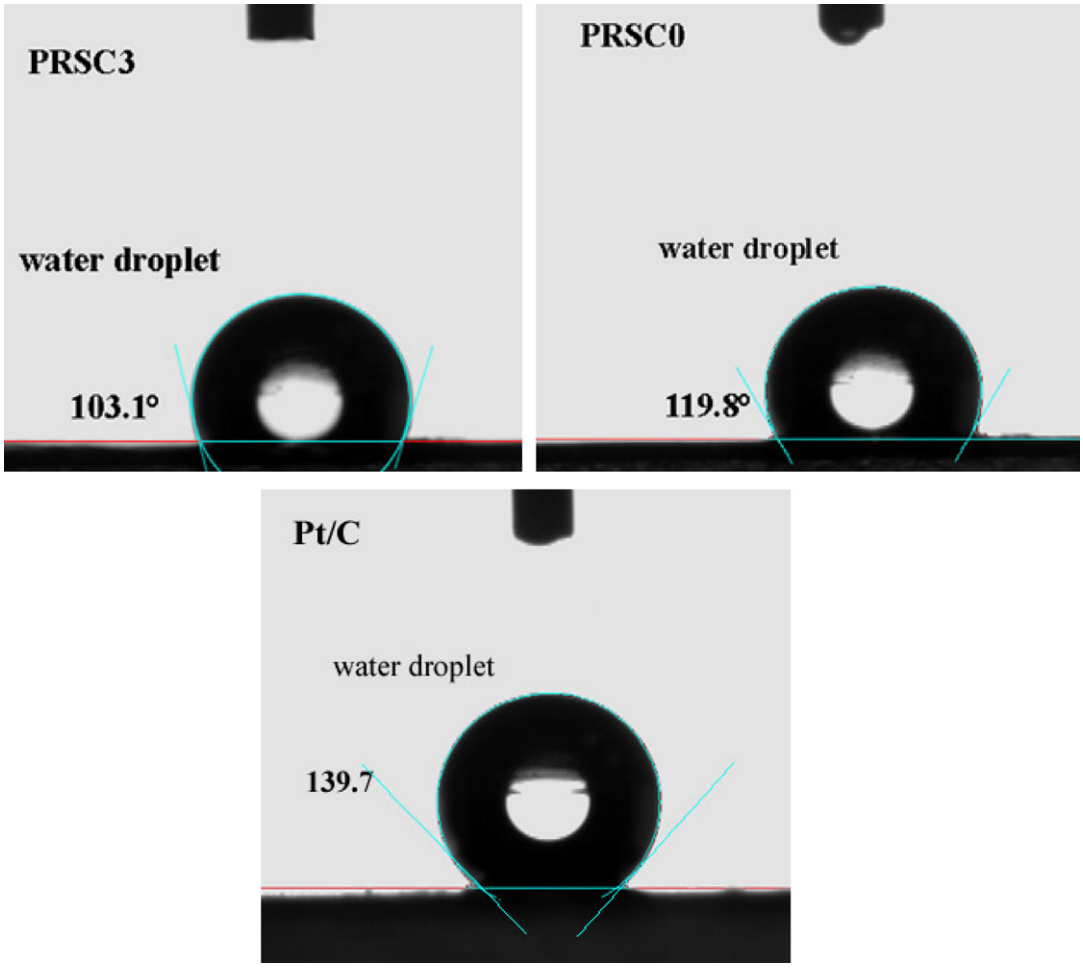

Fig. 4. Contact angles of MEAs measured using water droplets.

binding energy of Ru also increased significantly, implying that the binary oxide of silicon and ruthenium is not physically supported on the carbon support surface, but may be combined with carbon atoms via some chemical bonding; this is why we could not observed any silicon oxide particles on the surface of the carbon support.

Due to the dispersion of binary oxide on the carbon support, we speculated that the wettability of the catalyst may have increased, a possibility that was confirmed by the contact angle measurements. The contact angles of MEAs were shown in Fig. 4. For Pt/C catalyst, the contact angle was 139.7°, but for Pt/SiO_x/C the angle decreased to 119.8°, and for Pt/RuO_2–SiO_x/C (PRSC3), the angle further decreased to 103.1°. These results clearly reveal that the addition of ruthenium oxide significantly enhanced the wettability of Pt/RuO_2–SiO_x/C.

Cyclic voltammograms for Pt/SiO_x/C and Pt/RuO_2–SiO_x/C with different ruthenium oxide content in N_2-saturated 0.5 M H_2SO_4 are presented in Fig. 5. The number of Pt surface atoms was estimated from the charge associated with hydrogen desorption in the region of −0.20 to 0.1 V, using the stoichiometry of one adsorbed H atom per Pt atom. The electrochemical surface area (ECSA) in $m^2\ g^{-1}$ Pt was then calculated, assuming a correspondence value of 0.21 mC cm^{-2} Pt [27]. The ECSA of Pt/SiO_x/C was calculated to be 69.4 $m^2\ g^{-1}$ Pt. Fig. 5B shows that the ECSAs increased with increasing RuO_2 content (from 1 wt.% to 3 wt.%), then decreased (with 5 wt.%). A maximum ECSA of 91.8 $m^2\ g^{-1}$ (a 32% ECSA increase over PRSC0) was reached for PRSC3. Further increase in the doped RuO_2 content (to 5 wt.%) led to decreased ECSA, probably due to reduced support surface for Pt dispersion.

Fig. 6 shows the CVs of Pt/RuO_2–SiO_x/C catalysts with different RuO_2 content in H_2SO_4 + 0.50 M CH_3OH at room temperature. The current density in A mg^{-1} Pt reflects the mass activity of the catalysts for the methanol oxidation reaction. Compared with PRSC0, the Pt/RuO_2–SiO_x/C catalysts showed significant activity enhancement for methanol oxidation. The methanol oxidation activity for PRSC3 catalyst was about 0.52 A mg^{-1} Pt, which is 37% higher than that of the PRSC0 catalyst (0.38 A mg^{-1} Pt). The mass activity increase for PRSC3 (37%) is quite consistent with the ECSA increase (the ECSA increase of PRSC3 relative to PRSC0 is 32%), implying that the activity improvement may have resulted from the high dispersion of platinum caused by adding ruthenium oxide, but not the interaction of platinum with ruthenium or their synergistic effect. This suggestion is supported by the ratio of forward, i_f, to backward, i_b, anodic peak current density. As shown in Fig. 6, the ratio of i_f/i_b is almost unchanged with the addition of ruthenium

Table 1
XPS data of RuO_2–SiO_x/C (3 wt.% RuO_2) catalyst support and PRSC3.

Sample	Binding energy (eV)			
	Pt_{4f}	$Ru_{3p3/2}$	Si_{2p}	C_{1s}
Pt/RuO_2–SiO_x/C (PRSC3)	71.7/74.6	463.9	104.3	284.6
RuO_2–SiO_x/C	—	463.2	103.2	284.6
Ref. [26]	71.2/74.5	462.4[a]	101.9[b]	284.6

[a] RuO_2.
[b] SiO_x.

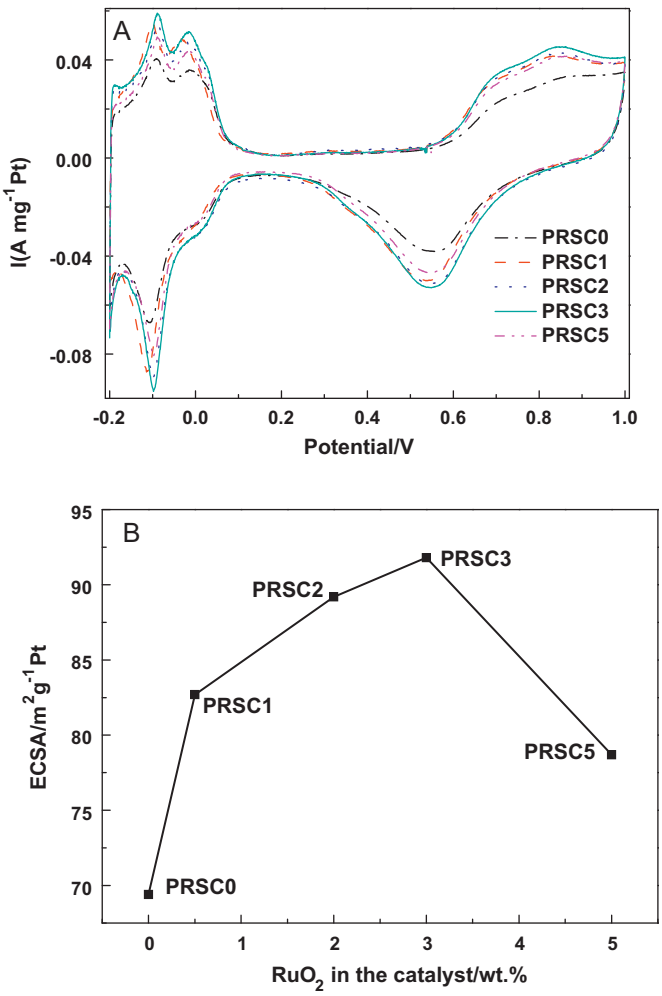

Fig. 5. (A) Cyclic voltammograms of Pt/RuO_2–SiO_2/C catalysts with different ruthenium oxide content in 0.50 M H_2SO_4 solution at room temperature and at a scan rate of 50 mV s^{-1} and (B) the calculated ESCAs with the change in RuO_2 content.

oxide. Meanwhile, it is widely recognized that the ratio of i_f/i_b for PtRu alloy catalyst could be high over 1.0 due to the improvement of ruthenium to the removal of oxidization mediate of methanol adsorbed on the platinum [28], the unaffected i_f/i_b ratio is probably an indication of no interaction between Pt and Ru.

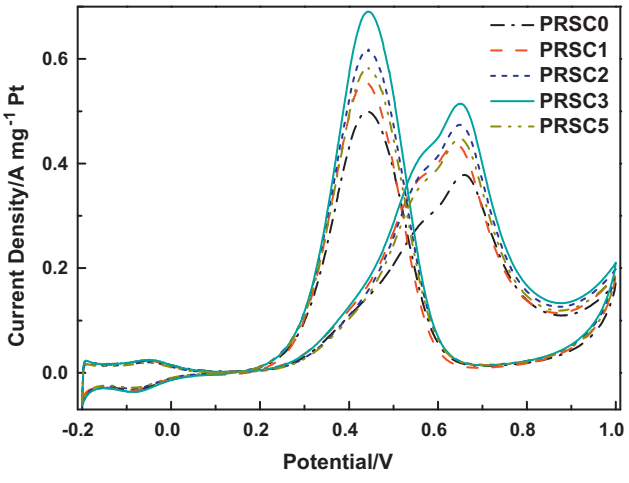

Fig. 6. Room temperature cyclic voltammograms of the catalysts in 0.50 M H_2SO_4 + 0.50 M CH_3OH at a scan rate of 50 mV s^{-1}.

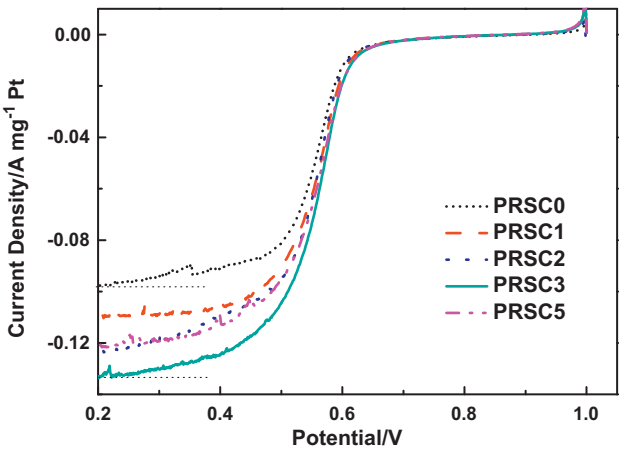

Fig. 7. Polarization curves for the oxygen reduction reaction in 0.5 M H_2SO_4 (saturated with pure O_2) at a sweep rate of 5 mV s^{-1} at room temperature (electrode rotating speed: 1600 rpm).

Polarization curves for the oxygen reduction reaction (ORR) measured in oxygen-saturated 0.50 M H_2SO_4 solution are recorded in Fig. 7. Considerable current density enhancement was found for all RuO_2-doped catalysts relative to Pt/SiO_2/C. The limiting current density increased in the order PRSC0 < PRSC1 < PRSC2 < PRSC3, whereas a slight activity decrease was registered for PRSC5 compared with PRSC3. The limiting current density of the PRSC3 catalyst is 39% higher than that of the PRSC0 catalyst. We believe that the activity increase for the ORR is again attributable to the better dispersion of Pt nanoparticles on the RuO_2-doped supports.

To test the self-humidification capability of the homemade catalyst, MEAs with different anode catalysts were fabricated and evaluated under identical conditions in a hydrogen–oxygen polymer exchange fuel cell test kit. Fig. 8 compares the MEA performance under non-humidified conditions. The MEAs were prepared using JM Pt/C catalyst (HiSPEC-4100) as the cathode and JM Pt/C, PRSC0, and PRSC3 as the respective anodes. Clearly, in the absence of any external gas humidification, the performance of the MEA prepared with the JM Pt/C anode catalyst decreased rapidly, the current density at 0.6 V dropping from 580 mA cm^{-2} to less than 400 mA cm^{-2} within 2 h. The current density for the MEA fabricated with the PRSC0 anode decreased from 640 mA cm^{-2} to ca. 590 mA cm^{-2} in the initial 3 h, then remained

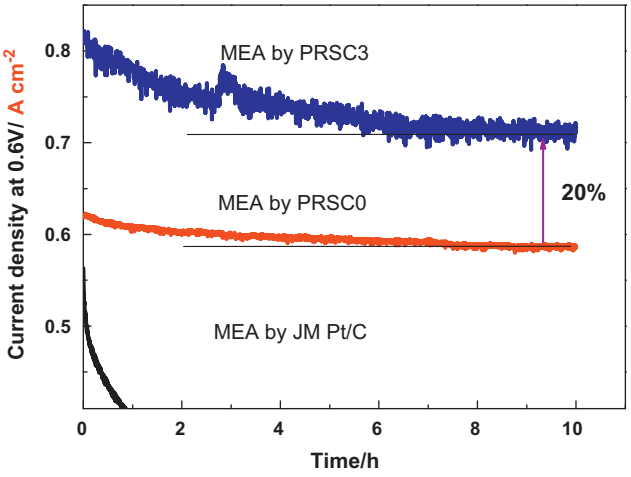

Fig. 8. MEA performance at 0.6 V in the absence of humidification (cell temperature: 50 °C; back-pressures for air and hydrogen: 20 psig; hydrogen and air flow rates: 300 and 800 ml min^{-1}, respectively).

quasi-stable at 590 mA cm^{-2} for at least 10 h. The best cell performance occurred with the MEA prepared using PRSC3: the current density at 0.6 V remained constant at 710 mA cm^{-2} for at least 10 h and showed a tendency to increase. Clearly, the MEAs fabricated with PRSC0 and PRSC3 displayed good self-humidification capability, but PRSC3 showed 20% higher performance due to the addition of RuO_2. The better self-humidification capability of PRSC3 relative to PRSC0 confirmed its superior wettability, as evidenced by the contact angle measurements mentioned above. And the higher self-humidification performance of PRSC3 compared to PRSC0 may result from the combination of its superior wettability and its high dispersion of platinum caused by the addition of ruthenium oxide, actually the enhancement of performance (20%) is consistent with the increase of ECSA (32%) in some extent.

4. Conclusions

$Pt/RuO_2–SiO_x/C$ electrocatalysts with different RuO_2 content were prepared and evaluated for the methanol oxidation and oxygen reduction reactions, and tested in a hydrogen-air single cell to determine their self-humidification capacities. The addition of RuO_2 significantly improved the dispersion of the active components (Pt nanoparticles), and 3 wt.% RuO_2 was found to be the optimal content. Compared with $Pt/SiO_x/C$, the $Pt/RuO_2–SiO_x/C$ catalyst with 3 wt.% RuO_2 showed activity enhancements of 37% and 39% for methanol oxidation and oxygen reduction, respectively. Furthermore, the MEAs prepared with $Pt/RuO_2–SiO_x/C$ as the anode catalyst showed better wettability and excellent self-humidification capability. The addition of RuO_2 was found to play multiple roles in the catalyst: on the one hand, it improved the dispersion of active components and enhanced catalytic activity; on the other hand, the wettability and self-humidification were significantly improved when $Pt/RuO_2–SiO_x/C$ was used as the anode catalyst of MEAs for a H_2-air fuel cell.

Acknowledgment

We would like to thank the National Scientific Foundation of China (NSFC Project Nos. 20876062 and 21076089) for financial support of this work.

References

[1] N. Rajalakshmi, S. Pandian, K.S. Dhathathreyan, Int. J. Hydrogen Energy 34 (2009) 3833.
[2] M. Oszcipok, M. Zedda, J. Hesselmann, M. Huppmann, M. Wodrich, M. Junghardt, C. Hebling, J. Power Sources 157 (2006) 666.
[3] W. Dai, H. Wang, X.Z. Yuan, J.J. Martin, D.J. Yang, J. Qiao, J.X. Ma, Int. J. Hydrogen Energy 34 (2009) 9461.
[4] T. Yang, Int. J. Hydrogen Energy 33 (2008) 2530.
[5] Y. Lee, B. Kim, Y. Kim, Int. J. Hydrogen Energy 34 (2009) 1999.
[6] C. Bi, H.M. Zhang, Y. Zhang, X.B. Zhu, Y.W. Ma, H. Dai, S.H. Xiao, J. Power Sources 184 (2008) 197.
[7] Y.H. Liu, T. Nguyen, N. Kristian, Y.L. Yu, X. Wang, J. Membr. Sci. 330 (2009) 357.
[8] Y.H. Liu, B.L. Yi, Z.G. Shao, L. Wang, D.M. Xing, H.M. Zhang, J. Power Sources 163 (2007) 807.
[9] W.J. Zhang, M.K.S. Li, P.L. Yue, P. Gao, Langmuir 24 (2008) 2663.
[10] H. Uchida, Y. Ueno, H. Hagihara, M. Watanabe, J. Electrochem. Soc. 150 (2003) A57.
[11] Y. Zhang, H.M. Zhang, Y.F. Zhai, X.B. Zhua, C. Bi, J. Power Sources 168 (2007) 323.
[12] Y. Zhang, H.M. Zhang, X.B. Zhu, C. Bi, J. Phys. Chem. B 111 (2007) 6391.
[13] D.H. Son, R.K. Sharma, Y.G. Shul, H.S. Kim, J. Power Sources 165 (2007) 733.
[14] Z.L. Miao, H.M. Yu, W. Song, D. Zhao, L.X. Hao, B.L. Yi, Z.G. Shao, Electrochem. Commun. 11 (2009) 787.
[15] W.K. Chao, C.M. Lee, D.C. Tsai, C.C. Chou, K.L. Hsueh, F.S. Shieu, J. Power Sources 185 (2008) 136.
[16] S. Vengatesan, H.-J. Kim, S.-Y. Lee, E. Cho, H. Yong Ha, I.-H. Oh, S.-A. Hong, T.-H. Lim, Int. J. Hydrogen Energy 33 (2008) 171.
[17] U.H. Jung, K.T. Park, E.H. Park, S.H. Kim, J. Power Sources 159 (2006) 529.
[18] U.H. Jung, S.U. Jeong, K.T. Park, H.M. Lee, K. Chun, D.W. Choi, Int. J. Hydrogen Energy 32 (2007) 4459.
[19] H.N. Su, L.M. Xu, H.P. Zhu, Y.N. Wu, L.J. Yang, S.J. Liao, H.Y. Song, Z.X. Liang, V. Birss, Int. J. Hydrogen Energy 35 (2010) 7874.
[20] H.N. Su, L.J. Yang, S.J. Liao, Q. Zeng, Electrochim. Acta 55 (2010) 8894.
[21] M.A. Worsley, J.D. Kuntz, J.H. Satcher, T.F. Baumann, J. Mater. Chem. 20 (2010) 4840.
[22] S.J. Liao, K.-A. Holmes, H. Tsaprailis, V.I. Birss, J. Am. Chem. Soc. 128 (2006) 3504.
[23] L.M. Xu, S.J. Liao, L.J. Yang, Z.X. Liang, Fuel Cells 9 (2009) 101.
[24] E. Antolini, F. Cardellini, J. Alloys Compd. 315 (2001) 118.
[25] R. Chetty, W. Xia, S. Kundu, M. Bron, T. Reinecke, W. Schuhmann, M. Muhler, Langmuir 25 (2009) 3853.
[26] XPS Database, http://srdata.nist.gov/xps.
[27] Y.K. Zhou, B.L. He, W.J. Zhou, J. Huang, X.H. Li, B. Wu, H.L. Li, Electrochim. Acta 49 (2004) 257.
[28] H.L. Gao, S.J. Liao, J.H. Zeng, Y.C. Xie, J. Power Sources 196 (2011) 54.